Research

Influence of model based iterative reconstruction algorithm on image quality of multiplanar reformations in reduced dose chest CT

Heloise Barras[1], Vincent Dunet[2], Anne-Lise Hachulla[2], Jochen Grimm[1] and Catherine Beigelman-Aubry[1]

Abstract

Background: Model-based iterative reconstruction (MBIR) reduces image noise and improves image quality (IQ) but its influence on post-processing tools including maximal intensity projection (MIP) and minimal intensity projection (mIP) remains unknown.

Purpose: To evaluate the influence on IQ of MBIR on native, mIP, MIP axial and coronal reformats of reduced dose computed tomography (RD-CT) chest acquisition.

Material and Methods: Raw data of 50 patients, who underwent a standard dose CT (SD-CT) and a follow-up RD-CT with a CT dose index (CTDI) of 2–3 mGy, were reconstructed by MBIR and FBP. Native slices, 4-mm-thick MIP, and 3-mm-thick mIP axial and coronal reformats were generated. The relative IQ, subjective IQ, image noise, and number of artifacts were determined in order to compare different reconstructions of RD-CT with reference SD-CT.

Results: The lowest noise was observed with MBIR. RD-CT reconstructed by MBIR exhibited the best relative and subjective IQ on coronal view regardless of the post-processing tool. MBIR generated the lowest rate of artefacts on coronal mIP/MIP reformats and the highest one on axial reformats, mainly represented by distortions and stairsteps artifacts.

Conclusion: The MBIR algorithm reduces image noise but generates more artifacts than FBP on axial mIP and MIP reformats of RD-CT. Conversely, it significantly improves IQ on coronal views, without increasing artifacts, regardless of the post-processing technique.

Introduction

Radiation exposure among the population has significantly increased these last decades, especially due to the raised diagnostic role of multidetector row computed tomography (CT) in patient management (1,2). The examinations must be performed using doses that are As Low As Reasonably Achievable (ALARA), consistent with the diagnostic task (3). In this way, iterative reconstruction (IR) algorithms that reduce image noise while improving overall image quality (IQ) when compared to filtered back projection (FBP) have been developed (4–7). One of them, model-based iterative

[1]Department of Radiodiagnostic and Interventional Radiology, Lausanne University Hospital, Lausanne, Switzerland
[2]Division of Radiology, Geneva University Hospital, Geneva, Switzerland

Corresponding author:
Heloise Barras, Department of Radiodiagnostic and Interventional Radiology, Lausanne University Hospital, Rue du Bugnon 46, CH-1011 Lausanne, Switzerland.
Email: Heloise.Barras@chuv.ch

reconstruction (MBIR), allows calculation of noise statistics and includes modelling of optical factors and exact geometric features of the cone beam and the absorbing voxels (4).

Post-processing tools including maximal intensity projection (MIP) and minimal intensity projection (mIP) have been proven useful for lung analysis (8–10). In routine practice, MIP is able to detect and evaluate the profusion of micronodules as well as to characterize them as centrilobular, perilymphatic, or with a miliary distribution (11). Additionally, mIP has been proven useful for any other infiltrative lung disease or to assess lung perfusion (11,12) while allowing an accurate assessment of the airways. Although the impact of the MBIR algorithm has been substantially described in the literature on native axial slices, the impact on the post-processing has not been evaluated yet, neither on axial nor on coronal orientation.

We thus aimed at performing a detailed evaluation of the impact of the MBIR algorithm on IQ and diagnostic confidence compared to FBP algorithm on axial and coronal native views, MIP and mIP reformats. Reference CT examination at standard dose (SD-CT) was compared to follow-up CT examination at reduced dose (RD-CT) reconstructed by FBP and MBIR. The term of RD-CT was preferred to the terms of low-dose or ultra-low dose, which are usually considered for a CT dose index (CTDI) of 2–3 mGy and <1 mGy, respectively, but remain controversial due to the evolving dose reduction processes.

Material and Methods

Study design

Chest CTs of 200 consecutive patients who underwent both a reference SD-CT and a follow-up RD-CT between January 2013 and July 2014 were retrospectively reviewed. Inclusion criteria were: participants aged older than 18 years; hemodynamically stable and able to hold breath for 5 s; without occurrence of any major event between SD-CT and RD-CT; a maximal delay between SD-CT and RD-CT of 2 years; SD-CT and RD-CT performed on the same CT-scanner in our institution; CTDI of 2–3 mGy for RD-CT. Pregnant patients were excluded from the study. One hundred and fifty patients were excluded from the analysis because SD-CT was performed more than 2 years before RD-CT (n = 81/150, 54%), on different CT scanners of other institutions using different acquisition or reconstruction parameters (n = 42/150, 29%) or because the CTDI of RD-CT was higher than 2–3 mGy (n = 27/150, 17%). Fifty consecutive patients (35 men; age, 53.9 ± 15.6 years) fulfilled the inclusion

criteria. RD-CT was requested for the follow-up of lung nodules (n = 17), infiltrative lung disease (n = 13), infectious disorders (n = 10), and other miscellaneous chest disorders (n = 10). Considering infiltrative lung disease, we included usual interstitial pneumonia, lymphocytic interstitial pneumonia, and non-specific interstitial pneumonia. All diagnoses were verified by consulting patients' files of the Department of Pulmonology of our institution.

This retrospective study was approved by our Institutional Ethic Committee, which waived the requirement for obtaining patient informed consent.

Scanning techniques and reconstruction

Chest CT acquisitions were performed using a helical 64-row CT-scanner (Discovery CT750HD, GE Healthcare, Milwaukee, WI, USA) without intravenous contrast agent. Scanning parameters for the RD-CT were held constant according to data of the literature (1,13,14) and to our practice with a CTDI of 2 or 3 mGy depending on the patient sex and morphology as follows: 2 mGy for women and 3 mGy for men or for any patient with BMI > 25 kg/m^2. Mean BMI value was 23.0 ± 4.3 kg/m^2. The following parameters were used: mean current tube, 90 mAs (this means a range of 10–90 mAs using current modulation with a noise index of 25); voltage tube, 100–120 kV depending of patient's BMI (100 kV when BMI < 25 kg/m^2 and 120 kV when BMI > 25 kg/m^2); pitch, 1.375 with a table speed of 55 mm/s; detector configuration, 64×0.625 mm; gantry rotation time, 0.6 s; matrix, 512×512; field of view, 50 cm.

Raw data were reconstructed by using 1.25-mm slice thickness every 0.6 mm with FBP with sharp kernel for the SD-CT studies, FBP with sharp and soft kernels, and MBIR for the follow-up RD-CT studies. Native slices as well as 3-mm thick mIP and 4-mm thick MIP reformats were performed on the axial and coronal planes to compare the different protocols of reconstruction.

Radiation dose assessment

For each patient and according to the literature (15), the volume CTDI (CTDIvol) and the dose length product (DLP) estimation were recorded for SD-CT studies. For follow-up studies, owing to the fact that the CTDI were predetermined, only DLP values were recorded. Effective dose was estimated by multiplying the DLP with the chest-specific conversion coefficient (0.017 mSv/mGy.cm). Size specific dose estimation (SSDE) was also calculated by multiplying CTDIvol with a conversion factor depending of the effective diameter (16).

Image reading

All CT studies were anonymized, randomly displayed and independently evaluated on the same workstation. Standard lung parenchymal (center, –600 HU; width, 1600 HU) and mediastinal (center, 40 HU; width, 400 HU) window settings were used by default. Readers were allowed to change magnification at their own convenience. The reading was focused on the right lung according to the less degree of kinetic artifacts compared to the left one.

Subjective image quality and artifacts analysis

For every patient, subjective IQ and artifacts were independently recorded by two radiologists (with 24 and 7 years of experience in thoracic imaging) according to European Guidelines (17). Each reconstruction series (SD-CT reconstructed by FBP with sharp kernel, RD-CT reconstructed by FBP with sharp kernel, soft kernel, and MBIR) was analyzed on native slices, mIP and MIP axial and coronal reformats. A total of 24 series by patient was thus evaluated.

For subjective IQ analysis evaluated independently for each series, a semi-quantitative five-point scale was used as follows: 1, best IQ with no artifacts; 2, good IQ with minimal artifacts; 3, moderate IQ with some artifacts; 4, low IQ with numerous artifacts but still interpretable; and 5, worst IQ not interpretable. Criteria of evaluation included the sharpness of normal structures such as fissures or lung-vessel margins on native images as well as the borders of the bronchi on mIP and of the vessels on MIP reformats, and also the potential penalty generated by the artifacts. The visualization of the most distal bronchi analyzable was also considered for evaluation of mIP reformats.

Artifacts were evaluated for each series with a two-point scale (0, absent; 1, present) by the two observers. They were classified in five categories as follows: stairsteps; blurred borders of bronchi on mIP reformations; blurred borders of vessels on MIP reformations; paravascular hypoattenuated bands; and distortion/elongated perception of the image details.

Objective image quality analysis

For every patient, circular regions of interest (ROI) were drawn in the ascending aorta and the trachea at the carina level on two successive slices. A size of $100 \pm 2\,mm^2$ with a constant position of each ROI was used throughout the entire study. The standard deviation of the mean attenuation values for each ROI served as objective measurements to estimate image noise according to the Miéville formula (18). Standard deviation measurements of the two successive slices were averaged and recorded for each of the 24 series described above.

Diagnostic confidence

To assess the impact of IQ on diagnostic confidence, relative IQ analysis was carried out. A semi-quantitative four-point scale was used as follows: 1 for the highest confident diagnosis to 4 for the most impaired diagnosis. Diagnostic confidence was compared between the reconstructions for each reformat. Moreover, inter-observer concordance was assessed according to the four main diagnoses of our study population: lung nodules (n = 17), infiltrative lung disease (n = 13), infectious disorders (n = 10), and miscellaneous (n = 10).

Statistical analysis

All statistics were performed with the Stata 13.1 software (StataCorp LP, College Station, TX, USA). Continuous variables are presented as mean $\pm$ SD and categorical variables as number. Subjective and objective IQs, artifacts, and relative IQ were compared between the different reconstruction protocols for each post-processing method using Kruskal–Wallis test. Post-hoc analysis was subsequently performed using the Wilcoxon test. Inter-observer concordance was assessed using the Lin's test that provides Pearson's correlation coefficient (rho, the measure of consistency), concordance correlation coefficient (rho_c, the measure of agreement), and the bias-correction factor ($Cb = rho_c/rho$) that measures the systematic bias. A P value < 0.001 was considered statistically significant after Bonferroni correction for multiple comparisons.

Results

Radiation dose

The mean CTDIvol for RD-CT was significantly lower than for SD-CT ($2.3 \pm 0.5\,mGy$ vs. $7.0 \pm 2.2\,mGy$, $P < 0.0001$). The mean SSDE for RD-CT was $3.1 \pm 0.6\,mGy.cm$ and $9.3 \pm 2.6\,mGy.cm$ for SD-CT ($P < 0.0001$). The mean effective dose was significantly lower for RD-CT than for SD-CT ($1.6 \pm 0.5\,mSv$ vs. $4.3 \pm 2.0\,mSv$, $P < 0.0001$).

Subjective image quality

All results are displayed in Table 1. For subjective IQ on axial views, SD-CT achieved the highest average score both on native slices ($P = 0.0001$) and MIP reformations ($P = 0.0001$). On mIP reformations, there was no significant difference between RD-CT reconstructed by MBIR and SD-CT ($P > 0.05$). However, on coronal

Table 1. Results for the evaluation of image quality.

Image quality	Plan	View	SD-CT FBP sharp kernel	RD-CT FBP sharp kernel	FBP soft kernel	MBIR	P value
Relative	Axial	Native	1.14 ± 0.45	$3.98 \pm 0.14^{*\dagger}$	$2.9 \pm 0.36^{*\dagger}$	$1.98 \pm 0.43^{*}$	0.0001
		miP	2.12 ± 0.90	$4.0 \pm 0.0^{*\dagger}$	$2.38 \pm 0.60^{\dagger}$	$1.5 \pm 0.68^{*}$	0.0001
		MIP	1.18 ± 0.56	$4.0 \pm 0.0^{*\dagger}$	$2.74 \pm 0.44^{*\dagger}$	$2.06 \pm 0.51^{*}$	0.0001
	Coronal	Native	2.58 ± 0.64	$3.96 \pm 0.20^{*\dagger}$	$2.4 \pm 0.53^{\dagger}$	$1.08 \pm 0.27^{*}$	0.0001
		miP	2.96 ± 0.40	$3.98 \pm 0.25^{*\dagger}$	$1.94 \pm 0.37^{*\dagger}$	$1.14 \pm 0.40^{*}$	0.0001
		MIP	2.56 ± 0.76	$3.98 \pm 0.14^{*\dagger}$	$2.3 \pm 0.46^{*\dagger}$	$1.18 \pm 0.44^{*}$	0.0001
Subjective	Axial	Native	1.62 ± 0.60	$3.16 \pm 0.51^{*\dagger}$	$2.3 \pm 0.51^{*}$	$2.18 \pm 0.48^{*}$	0.0001
		miP	1.96 ± 0.40	$2.86 \pm 0.45^{*\dagger}$	2.08 ± 0.44	1.88 ± 0.48	0.0001
		MIP	1.86 ± 0.40	$3.26 \pm 0.63^{*\dagger}$	$2.44 \pm 0.58^{*}$	$2.3 \pm 0.51^{*}$	0.0001
	Coronal	Native	2.64 ± 0.69	$3.6 \pm 0.67^{*\dagger}$	$2.56 \pm 0.54^{\dagger}$	$1.78 \pm 0.51^{*}$	0.0001
		miP	2.94 ± 0.62	$3.46 \pm 0.58^{*\dagger}$	$2.22 \pm 0.46^{*}$	$1.8 \pm 0.57^{*}$	0.0001
		MIP	2.68 ± 0.55	$3.66 \pm 0.63^{*\dagger}$	$2.56 \pm 0.54^{\dagger}$	$2.06 \pm 0.59^{*}$	0.0001
Objective, noise (HU)	Axial	Native	54 ± 26	$89 \pm 38^{*\dagger}$	$26 \pm 10^{*\dagger}$	$11 \pm 3^{*}$	0.0001
		miP	42 ± 13	$69 \pm 21^{*\dagger}$	$20 \pm 6^{*\dagger}$	$9 \pm 2^{*}$	0.0001
		MIP	43 ± 13	$71 \pm 21^{*\dagger}$	$21 \pm 10^{*\dagger}$	$9 \pm 2^{*}$	0.0001
	Coronal	Native	50 ± 20	$84 \pm 25^{*\dagger}$	$25 \pm 7^{*\dagger}$	$11 \pm 2^{*}$	0.0001
		miP	36 ± 10	$61 \pm 16^{*\dagger}$	$19 \pm 5^{*\dagger}$	$10 \pm 2^{*}$	0.0001
		MIP	35 ± 10	$59 \pm 16^{*\dagger}$	$19 \pm 6^{*\dagger}$	$10 \pm 4^{*}$	0.0001

P values on the right column are given for comparison by Kruskal–Wallis test.
*For post-hoc comparisons to SD-CT with Wilcoxon test, $P < 0.001$.
$\dagger$For post-hoc comparisons to MBIR with Wilcoxon test, $P < 0.001$.
CT, computed tomography; FBP, filtered back projection; HU, Hounsfield unit; MBIR, model-based iterative reconstruction; SD, standard dose.

views, MBIR had a significant higher IQ than the three other reconstruction protocols regardless of the post-processing tool used ($P < 0.0002$).

Evaluation of inter-observer concordance is reported in Supplementary Table 1. Overall, the concordance between the two readers was good for subjective IQ scoring (rho $= 0.72$, $rho_c = 0.71$, $Cb = 0.99$). Taking into account all series separately, regardless of the diagnosis, inter-observer concordance was better with MBIR than with FBP on RD-CT but worse than with SD-CT.

Objective image quality

Image noise was the greatest for the RD-CT reconstructed by FBP with sharp kernel, and the lowest for the RD-CT reconstructed by MBIR both for axial and coronal planes regardless of the post-processing tool ($P < 0.0001$). Details are displayed in Table 1.

Artifacts

Artifacts analysis on native slices is displayed in Supplementary Table 2. On axial views, MBIR exhibited more distortions and RD-CT reconstructed by FBP with soft kernel presented more blurred bronchi and vessels than the two other protocols. On coronal views, MBIR exhibited more blurred bronchi than SD-CT and more stairsteps than RD-CT reconstructed by FBP with soft kernel.

Results for artifacts analyses on mIP and MIP are displayed in Table 2. Overall, there was no significant difference between protocols using axial mIP ($P = 0.54$) and coronal MIP reformats ($P = 0.25$). On axial MIP reformats, RD-CT reconstructed by MBIR exhibited more stairsteps and distortions than the SD-CT. On coronal mIP reformats, RD-CT reconstructed by MBIR exhibited a lower number of artifacts than the SD-CT, especially regarding paravascular hypoattenuated bands.

Inter-observer concordance was good for blurred bronchi (rho $= 0.70$, $rho_c = 0.70$, $Cb = 1.0$), blurred vessels (rho $= 0.76$, $rho_c = 0.76$, $Cb = 0.99$), hypoattenuated paravascular bands (rho $= 0.76$, $rho_c = 0.75$, $Cb = 0.99$) and distortion (rho $= 0.72$, $rho_c = 0.71$, $Cb = 0.99$), and moderate (rho $= 0.45$, $rho_c = 0.44$, $Cb = 0.97$) for stairsteps artifacts.

Table 2. Comparison of artifacts on reformatted images.

Plan	Reformat	Artifacts	SD-CT FBP sharp kernel	RD-CT FBP sharp kernel	FBP soft kernel	MBIR	P value
Axial	mIP	Stepstairs	7	9	I	I2	0.25
		Blurred bronchi	I	0[†]	3I*[†]	I5*	0.0001
		Blurred vessels	0	0	5	0	0.76
		Paravascular hypoattenuated bands	32	30[†]	4*	0*	0.0001
		Distortion	0	I[†]	I[†]	23*	0.0001
		All	40	40	42	50	0.54
	MIP	Stepstairs	4	I2	2[†]	23*	0.0006
		Blurred bronchi	0	0	5	2	0.79
		Blurred vessels	0	2[†]	39*[†]	I4*	0.0001
		Paravascular hypoattenuated bands	I	0	0	0	1.0
		Distortion	0	0	0[†]	I9*	0.0006
		All	5	I4[†]	46*	58*	0.0001
Coronal	mIP	Stepstairs	23	30	4*[†]	26	0.0001
		Blurred bronchi	0	0	35*[†]	7	0.0001
		Blurred vessels	I	I	3	0	0.96
		Paravascular hypoattenuated bands	3I	25[†]	I*	0*	0.0001
		Distortion	0	0	0	0	1.0
		All	55	56	43	33*	0.002
	MIP	Stepstairs	35	38	2*[†]	30	0.0001
		Blurred bronchi	0	0	3	0	0.93
		Blurred vessels	2	I	4I*[†]	5	0.0001
		Paravascular hypoattenuated bands	I	0	0	0	0.99
		Distortion	0	0	0	0	1.0
		All	38	39	46	35	0.25

P values on the right column are given for comparison by Kruskal–Wallis test.
*For post-hoc comparisons to SD-CT with Wilcoxon test, $P < 0.001$.
[†]For post-hoc comparisons to MBIR with Wilcoxon test, $P < 0.001$.
CT, computed tomography; FBP, filtered back projection; MBIR, model-based iterative reconstruction; SD, standard dose.

Diagnostic confidence

Regarding the relative IQ of axial views, SD-CT received the highest average rank both for native slices and MIP reformations ($P = 0.0001$) while MBIR obtained the highest rank for mIP reformations ($P = 0.0001$, Fig. 1). For coronal views, RD-CT reconstructed by MBIR received the highest average rank ($P = 0.0001$) (Figs. 1 and 2) whatever the post-processing technique used (Fig. 3).

Overall, the concordance between the two readers was good for relative IQ scoring (rho = 0.89, rho$_c$ = 0.89, Cb = 1.0). However, for axial views, in patients with infiltrative lung disease, inter-observer concordance for the diagnostic confidence was lower with MBIR (rho = 0.49, rho$_c$ = 0.44, Cb = 0.9) than with SD-CT (rho = 0.70, rho$_c$ = 0.68, Cb = 0.98). Inter-observer concordance for the diagnostic confidence was also lower in patients with infectious disease using MBIR (rho = 0.45, rho$_c$ = 0.39, Cb = 0.87 for MBIR, and rho = 0.68, rho$_c$ = 0.66, Cb = 0.96 for SD-CT). For coronal views, inter-observer concordance for the diagnostic confidence did not change according to patients' diagnoses.

Discussion

The impact on IQ of IR algorithms on native axial slices has been largely described in the literature.
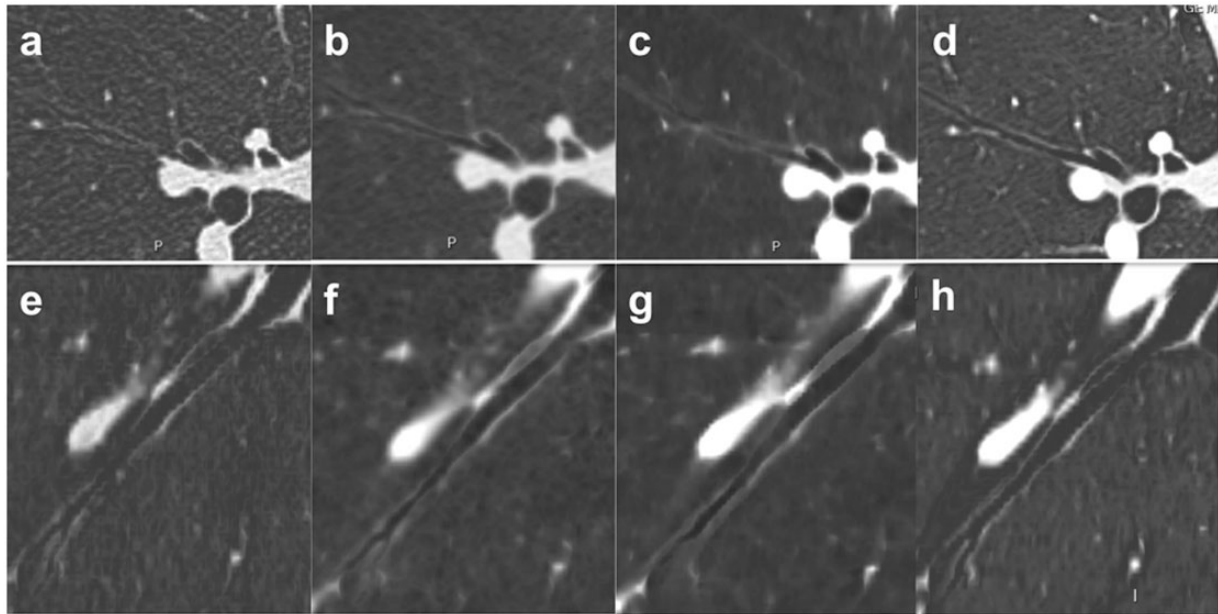
Fig. 1. 3-mm thick mIP reformats on axial (top line) and coronal views (bottom line) for reconstruction of RD-CT by FBP with sharp kernel (a, e), RD-CT by FBP with soft kernel (b, f), RD-CT by MBIR (c, g), and SD-CT by FBP with sharp kernel (d, h). On mIP axial views, the highest quality was obtained with RD-CT reconstructed by MBIR (c) followed by SD-CT (d) and RD-CT reconstructed by FBP with soft kernel (b) and sharp kernel (a). On coronal views, the highest quality was obtained with MBIR (g) followed by RD-CT with soft kernel (f), SD-CT (h), and RD-CT with sharp kernel (e). Note in this case that the bronchial wall is much better delineated on coronal than on axial view with MBIR. On axial view, the wall of the bronchi appeared thickened and less well delineated from the bronchial lumen with MBIR (c). Note the stairsteps artifacts on coronal view reconstructed by FBP with sharp kernel either at reduced dose (e) or standard dose (h), also seen with MBIR (g) but not on RD-CT reconstructed by FBP with soft kernel (f).
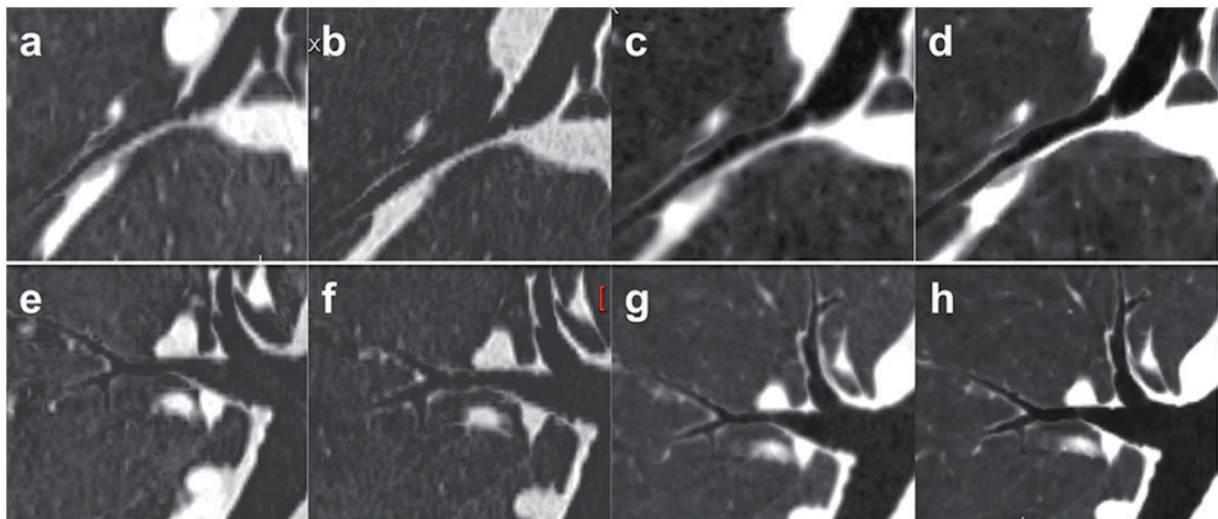

Fig. 2. 3-mm thick mIP reformats on coronal views focusing on inferior (top line) and superior (bottom line) right lobar bronchus for reconstruction of SD-CT by FBP with sharp kernel (a, e), RD-CT by FBP with sharp kernel (b, f), RD-CT by FBP with soft kernel (c, g), and RD-CT by MBIR (d, h). Note the stairsteps artifacts mostly pronounced on SD-CT (a, e) and RD-CT reconstructed by FBP with sharp kernel (b, f). The gain in the sharpness of bronchial wall thickness overtakes the minimal stairsteps artifacts with MBIR (d, h) compared with RD-CT reconstructed by FBP with soft kernel (c, g). The MBIR reconstruction was classified with the highest IQ.
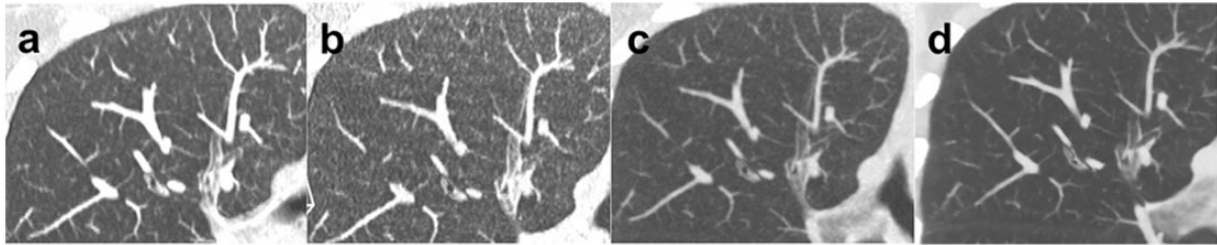
Fig. 3. 4-mm thick MIP reformats on coronal views focusing on right upper lobe for reconstruction of SD-CT by FBP with sharp kernel (a), RD-CT by FBP with sharp kernel (b), RD-CT by FBP with soft kernel (c), and RD-CT by MBIR (d). The best image quality was obtained with RD-CT reconstructed by MBIR (d) followed by RD-CT reconstructed by FBP with soft kernel. Note the lesser diagnostic confidence with SD-CT (a) and RD-CT reconstructed by FBP with sharp kernel due to the rendering artificial micronodules simulating micronodules, while RD-CT reconstructed by MBIR (d) showed no micronodules.

We hereby report the first study evaluating the influence of the MBIR algorithm on mIP and MIP either on axial or coronal planes. The main findings are: (i) the MBIR algorithm reduces image noise level but does not improve relative or subjective IQ on axial reformats; (ii) the MBIR algorithm generates more artifacts than FBP on axial views with mIP and MIP post-processing techniques; (iii) on coronal views, the MBIR algorithm significantly improves IQ without generating artifacts, regardless of the reformation type.

On axial views, numerous studies demonstrated that IR improves IQ and reduces noise level on native slices in different pulmonary diseases (14,19–31). In the present study, the MBIR algorithm significantly reduced noise level on native images as well as on mIP and MIP reformations compared to both SD-CT and RD-CT reconstructed by FBP with soft and sharp kernels, which concurs with current literature and extends it for reformats. Compared to SD-CT, the relative and subjective IQ of native RD-CT axial slices were however not improved by the MBIR algorithm, also confirming previous literature (19,23,30). Our study moreover extends this result for MIP and mIP reformats for which MBIR did not improve IQ. Nevertheless, compared to RD-CT reconstructed by FBP, the diagnostic confidence with axial native slices, MIP and mIP reformats was better for MBIR reconstructions. This reinforces the fact that MIP reformations of RD-CT reconstructed by FBP should be used with caution faced with tricky situations. Overall, while the MBIR algorithm reduced noise level, it did not outclass SD-CT on axial native or reformatted views.

To our knowledge, no study specifically evaluated the impact of the MBIR algorithm on coronal MIP/mIP reformats. On coronal views, the subjective and relative IQ of MBIR obtained the highest rank for native, mIP and MIP reformats. Taking into account that MBIR exhibited the lowest image noise, this reinforces the deleterious effect of the noise in the overall

IQ, which may simulate a miliary appearance (Fig. 3). In the same vein, RD-CT reconstructed by FBP with soft kernel had a better IQ on coronal mIP reformats compared to SD-CT and a significant lower noise level. This has to be linked to the decrease of noise level observed when using the soft kernel instead of the sharp one generated by the increase in voxel size despite the loss of spatial resolution (13). Overall, on coronal views, MBIR thus outclassed other reconstruction protocols on native slices, mIP and MIP reformats, which extends the current literature.

Regarding artifacts, already mentioned as "plastic appearance" by Kligerman et al. (31), MBIR exhibited more distortions and stairsteps on axial mIP and MIP reformats. Similar observations were reported when comparing MBIR to other algorithms in axial single slices of RD-CT (14,20). This may potentially prevent to a correct recognition of small details such as micronodules and/or tree-in-bud appearance, and can explain why diagnostic confidence (i.e. relative IQ) was lower on axial MIP reformats reconstructed with MBIR than SD-CT, despite noise reduction. Although inter-observer concordance for judging presence of artifacts was good for blurred bronchi, blurred vessels, hypoattenuated paravascular bands and distortion, it was moderate for stairsteps artifacts. The less obvious assessment of stairsteps artifacts compared with distortion could be linked to the not well-established definition of these artifacts.

The relative IQ comparison between the reconstructions for each reformat was based on the presumed perception of diagnostic confidence for the radiologists faced with the potentially most difficult diagnoses encountered in routine practice. We thus observed that inter-observer concordance decreased using MBIR axial views compared to SD-CT axial views in patients with infiltrative or infectious lung disease but not with lung nodules. As discussed above, the MBIR algorithm reduced image noise but generated more artifacts on axial views, which could have impaired

inter-observer concordance. This may indicate that, in patients with suspected disease that is characterized by subtle radiological signs such as infiltrative lung disease, axial images reconstructed by MBIR should not be read without coronal views to ensure diagnostic confidence and reproducibility. This point needs however to be confirmed in a larger cohort of patients with infiltrative lung disease.

There were some limitations in our study. First, the reference SD-CT was sometimes obtained with a long delay compared with the RD-CT exam until 2 years before. However, among the criteria of inclusion, a radiologist not involved in the reading selected studies without major event between SD-CT and RD-CT. Second, the results of this study concerned a specific IR algorithm. Although noise level reduction and improvement of IQ have been reported with MBIR compared to adaptive statistical iterative reconstruction algorithm on axial single slices of RD-CT (23), we cannot speculate if these results could be considered as valid on mIP/MIP reformats or using others algorithms of various equipments and companies. Third, the impact of MBIR on the diagnostic accuracy of RD-CT for infiltrative lung disease should be assessed in a larger cohort.

In conclusion, MBIR significantly reduces image noise but does not improve IQ due to the generation of artifacts, especially distortion and stairsteps on axial reformations of chest RD-CT. Compared to chest SD-CT, MBIR algorithm significantly improves both image noise and quality of coronal RD-CT views, without additional artifacts, regardless of the post-processing tool. The consequences of MBIR algorithm on axial IQ should be known for routine interpretation of chest RD-CT, notably when infiltrative lung disease is suspected.

References

1. Bankier AA, Tack D. Dose reduction strategies for thoracic multidetector computed tomography: background, current issues, and recommendations. J Thorac Imaging 2010;25:278–288.

2. Rogers LF. Radiation exposure in CT: why so high? Am J Roentgenol 2001;177:277.

3. McCollough CH, Primak AN, Braun N, et al. Strategies for reducing radiation dose in CT. Radiol Clin North Am 2009;47:27–40.

4. Fleischmann D, Boas FE. Computed tomography–old ideas and new technology. Eur Radiol 2011;21:510–517.

5. Baumueller S, Winklehner A, Karlo C, et al. Low-dose CT of the lung: potential value of iterative reconstructions. Eur Radiol 2012;22:2597–2606.

6. Mieville FA, Gudinchet F, Brunelle F, et al. Iterative reconstruction methods in two different MDCT scanners: physical metrics and 4-alternative forced-choice detectability experiments–a phantom approach. Phys Med 2013;29:99–110.

7. Singh S, Khawaja RD, Pourjabbar S, et al. Iterative image reconstruction and its role in cardiothoracic computed tomography. J Thorac Imaging 2013;28:355–367.

8. Kawel N, Seifert B, Luetolf M, et al. Effect of slab thickness on the CT detection of pulmonary nodules: use of sliding thin-slab maximum intensity projection and volume rendering. Am J Roentgenol 2009;192:1324–1329.

9. Kilburn-Toppin F, Arthurs OJ, Tasker AD, et al. Detection of pulmonary nodules at paediatric CT: maximum intensity projections and axial source images are complementary. Pediatr Radiol 2013;43:820–826.

10. Rampinelli C, Origgi D, Vecchi V, et al. Ultra-low-dose CT with model-based iterative reconstruction (MBIR): detection of ground-glass nodules in an anthropomorphic phantom study. Radiol Med 2015;120:611–617.

11. Beigelman-Aubry C, Hill C, Guibal A, et al. Multi-detector row CT and postprocessing techniques in the assessment of diffuse lung disease. Radiographics 2005;25:1639–1652.

12. Hayabuchi Y, Inoue M, Watanabe N, et al. Minimum-intensity projection of multidetector-row computed tomography for assessment of pulmonary hypertension in children with congenital heart disease. Int J Cardiol 2011;149:192–198.

13. Nakajo C, Heinzer S, Montandon S, et al. Chest CT at a dose below 0.3 mSv: impact of iterative reconstruction on image quality and lung analysis. Acta Radiol 2016;57:311–317.

14. Padole A, Singh S, Ackman JB, et al. Submillisievert chest CT with filtered back projection and iterative reconstruction techniques. Am J Roentgenol 2014;203:772–781.

15. Bankier AA, Kressel HY. Through the Looking Glass revisited: the need for more meaning and less drama in the reporting of dose and dose reduction in CT. Radiology 2012;265:4–8.

16. Leng S, Shiung M, Duan X, et al. Size-specific dose estimates for chest, abdominal, and pelvic CT: effect of intra-patient variability in water-equivalent diameter. Radiology 2015;277:308–309.

17. EUR16262. European guidelines on quality criteria for computed tomography. Available at: http://www.drs.dk/guidelines/ct/quality/ (accessed July 2015).

18. Mieville FA, Gudinchet F, Rizzo E, et al. Paediatric cardiac CT examinations: impact of the iterative

reconstruction method ASIR on image quality–preliminary findings. Pediatr Radiol 2011;41:1154–1164.

19. Vardhanabhuti V, Loader RJ, Mitchell GR, et al. Image quality assessment of standard- and low-dose chest CT using filtered back projection, adaptive statistical iterative reconstruction, and novel model-based iterative reconstruction algorithms. Am J Roentgenol 2013;200: 545–552.

20. Katsura M, Matsuda I, Akahane M, et al. Model-based iterative reconstruction technique for radiation dose reduction in chest CT: comparison with the adaptive statistical iterative reconstruction technique. Eur Radiol 2012;22:1613–1623.

21. Deak Z, Grimm JM, Treitl M, et al. Filtered back projection, adaptive statistical iterative reconstruction, and a model-based iterative reconstruction in abdominal CT: an experimental clinical study. Radiology 2013;266: 197–206.

22. Xu Y, He W, Chen H, et al. Impact of the adaptive statistical iterative reconstruction technique on image quality in ultra-low-dose CT. Clin Radiol 2013;68:902–908.

23. Ichikawa Y, Kitagawa K, Nagasawa N, et al. CT of the chest with model-based, fully iterative reconstruction: comparison with adaptive statistical iterative reconstruction. BMC Med Imaging 2013;13:27.

24. Annoni AD, Andreini D, Pontone G, et al. Ultra-low-dose CT for left atrium and pulmonary veins imaging using new model-based iterative reconstruction algorithm. Eur Heart J Cardiovasc Imaging 2015;16: 1366–1373.

25. Haggerty JE, Smith EA, Kunisaki SM, et al. CT imaging of congenital lung lesions: effect of iterative reconstruction on diagnostic performance and radiation dose. Pediatr Radiol 2015;45:989–997.

26. Neroladaki A, Botsikas D, Boudabbous S, et al. Computed tomography of the chest with model-based iterative reconstruction using a radiation exposure similar to chest X-ray examination: preliminary observations. Eur Radiol 2013;23:360–366.

27. Mathieu KB, Ai H, Fox PS, et al. Radiation dose reduction for CT lung cancer screening using ASIR and MBIR: a phantom study. J Appl Clin Med Phys 2014;15:4515.

28. Choo JY, Goo JM, Lee CH, et al. Quantitative analysis of emphysema and airway measurements according to iterative reconstruction algorithms: comparison of filtered back projection, adaptive statistical iterative reconstruction and model-based iterative reconstruction. Eur Radiol 2014;24:799–806.

29. Li K, Tang J, Chen GH. Statistical model based iterative reconstruction (MBIR) in clinical CT systems: experimental assessment of noise performance. Med Phys 2014;41:041906.

30. Montet X, Hachulla AL, Neroladaki A, et al. Image quality of low mA CT pulmonary angiography reconstructed with model based iterative reconstruction versus standard CT pulmonary angiography reconstructed with filtered back projection: an equivalency trial. Eur Radiol 2015;25:1665–1671.

31. Kligerman S, Lahiji K, Weihe E, et al. Detection of pulmonary embolism on computed tomography: improvement using a model-based iterative reconstruction algorithm compared with filtered back projection and iterative reconstruction algorithms. J Thorac Imaging 2015;30:60–68.